

Navier-Stokes/Forchheimer models for filtration through porous media

F. Cimolin^a, M. Discacciati^{b,*}

^a*Politecnico di Torino, Corso Duca degli Abruzzi 24, I-10129 Torino, Italy.*

^b*Laboratori de Càlcul Numèric (LaCàN), Escola Tècnica Superior d'Enginyers de Camins, Canals i Ports de Barcelona (ETSECCPB), Universitat Politècnica de Catalunya (UPC BarcelonaTech), Campus Nord UPC - C2, E-08034 Barcelona, Spain.*

Abstract

Modeling the filtration of incompressible fluids through porous media requires dealing with different types of partial differential equations in the fluid and porous subregions of the computational domain. Such equations must be coupled through physically significant continuity conditions at the interface separating the two subdomains. To avoid the difficulties of this heterogeneous approach, a widely used strategy is to consider the Navier-Stokes equations in the whole domain and to correct them introducing suitable terms that mimic the presence of the porous medium. In this paper we discuss these two different methodologies and we compare them numerically on a sample test case after proposing an iterative algorithm to solve a Navier-Stokes/Forchheimer problem. Finally, we apply these strategies to a problem of internal ventilation of motorbike helmets.

Keywords: Navier-Stokes equation, porous media flows, Darcy law, Forchheimer equation, penalization method, finite elements.

1. Introduction

2 In this paper we consider the modeling and numerical simulation of incom-
3 pressible fluid flows in regions partially occupied by porous media. The driving

*Corresponding author. Phone: 0034 93 401 0894, fax: 0034 93 401 1825.

Email addresses: flavio.cimolin@polito.it (F. Cimolin), marco.discacciati@upc.edu (M. Discacciati)

4 motivation of this work comes from a specific industrial problem of internal
5 ventilation for motorcycle helmets. However, problems associated with filtra-
6 tion of fluids in porous media have many other applications from geophysics to
7 engineering and also physiology. Consider for example the percolation of water
8 in hydrological basins through rocks or sand, the filtration of biofluids through
9 living tissues, as well as industrial processes involving fluids going through filters
10 and foams.

11 The problem of industrial interest discussed in this work, which will be
12 precisely described in Section 5, consists in modeling and simulating the internal
13 air flow of a motorcycle helmet. A series of intakes and outtakes connected by
14 channels dug into the protection layer let the fresh air enter the helmet and
15 filtrate through the comfort tissue and the hair of the rider. An appropriate
16 ventilation capable of effectively removing the heat and moisture produced by
17 the head must be guaranteed in order to preserve the safety of the rider even in
18 very hot and humid climates.

19 This work, which focuses only on the fluid-dynamics aspects of the air flow,
20 aims at investigating the possible modeling approaches for the physical descrip-
21 tion of the system, and it represents a preliminary step towards a more complex
22 model taking into account heat and sweat-related phenomena too (see [11]). In
23 spite of the specific application, most of the considerations associated with both
24 modeling and numerical simulation that will be discussed throughout the paper
25 are valid in the more general framework of flow over saturated porous media.

26 Due to the physical heterogeneity of the domain, a correct physical modeling
27 of filtration processes would require to introduce different systems of partial
28 differential equations in the free fluid domain and in the porous medium region,
29 giving rise to an heterogeneous differential system.

30 While for the vast majority of applications the Navier-Stokes equations rep-
31 resent the model to describe incompressible flows in the free-fluid region, the
32 modeling of flows through a saturated porous medium may require different
33 models depending on the characteristics of the porous medium itself. A classi-
34 cal model is given by the Darcy law [18], the simplest linear relation between the

35 velocity and the pressure. However, in case of high permeabilities the nonlinear
36 Forchheimer equation [25] is usually adopted.

37 A crucial issue in the definition of these heterogeneous models is the choice
38 of suitable coupling conditions to describe the fluid flow across the surface of
39 the porous medium through which the filtration occurs.

40 Those coupled problems have received an increasing attention during the last
41 years from both the mathematical and the numerical point of view. Starting
42 from the original experimental works of Beavers and Joseph on the coupling
43 conditions between a fluid and a porous medium, mathematical investigations
44 have been carried out in [22, 36, 37, 38, 41, 42]. Under those conditions, the
45 analysis of a coupled Stokes/Darcy problem has been studied in [10, 17, 19, 20,
46 28, 29, 26, 27, 30, 40, 48] in the steady case, and in [12, 53] in the time-dependent
47 case. Moreover, the case of the Navier-Stokes equations has been considered in
48 [3, 14, 19, 31].

49 However, because of the difficulties associated to the set-up and implemen-
50 tation of those models, a different approach is widely used in many practical
51 applications and it is implemented in most commercial softwares. This method,
52 often called penalization approach (see, e.g., [9, 34, 35, 39]), consists in consid-
53 ering in the whole computational domain a modified formulation of the Navier-
54 Stokes equations which reduce to their classical form in the fluid region while
55 they include additional resistance terms in the porous region. This approach is
56 similar to the so-called fictitious domain method [1, 39].

57 In this paper we compare these two different techniques studying their math-
58 ematical formulation and their finite element approximation. In particular, the
59 paper is organized as follows. In Section 2, we present the differential models
60 for the fluid flow as well as for the saturated porous media flow, we discuss
61 the coupling conditions for the heterogeneous case and we introduce suitable
62 adimensional formulations. In Section 3, we consider the numerical approx-
63 imation and we introduce possible solution strategies for the space-time dis-
64 cretization of these problems. Numerical results for the heterogeneous Navier-
65 Stokes/Forchheimer model are presented in Section 4, which includes also a

66 comparison of the simulation results obtained by the other modeling approaches.
 67 Finally, in Section 5 we show an example of application of the penalization
 68 method to the problem of internal ventilation of a helmet.

69 2. Mathematical models for the flow over a porous medium

70 We consider a bounded domain $\Omega \subset \mathbb{R}^d$ ($d = 2, 3$) partitioned into two non-
 71 overlapping regions: $\overline{\Omega} = \overline{\Omega}_f \cup \overline{\Omega}_p$, $\Omega_f \cap \Omega_p = \emptyset$, where Ω_f is the fluid domain
 72 (for example occupied by air or water) and Ω_p the saturated porous medium
 73 domain. We indicate by $\Gamma = \overline{\Omega}_f \cap \overline{\Omega}_p$ the interface between the two domains
 74 (see Figure 1). From the physical point of view, Γ represents the contact surface
 75 between the porous medium and the free fluid.

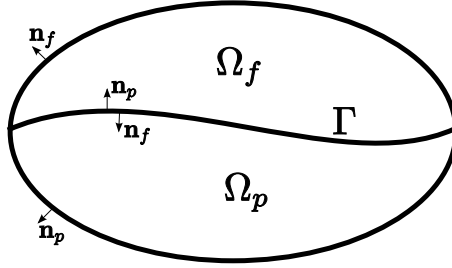


Figure 1: Subdivision of the computational domain Ω in a fluid region Ω_f and a porous domain Ω_p .

76 2.1. Fluid domain: the Navier-Stokes equations

77 In the fluid region Ω_f , we consider a confined incompressible viscous fluid
 78 modeled by the Navier-Stokes equations: for all $t > 0$,

$$\begin{aligned} \rho \left(\frac{\partial \mathbf{u}_f}{\partial t} + (\mathbf{u}_f \cdot \nabla) \mathbf{u}_f \right) - \mu \Delta \mathbf{u}_f + \nabla p_f &= \mathbf{0} && \text{in } \Omega_f, \\ \nabla \cdot \mathbf{u}_f &= 0 && \text{in } \Omega_f, \end{aligned} \quad (1)$$

79 where \mathbf{u}_f and p_f denote respectively the velocity and the pressure of the fluid,
 80 ρ and μ are respectively the density and dynamic viscosity of the fluid and we
 81 assume that no external body forces are applied.

82 We have denoted by ∇ , $\nabla \cdot$ and Δ , respectively, the gradient, the divergence
 83 and the Laplace operators with respect to the space coordinates. Moreover,
 84 we recall that $(\mathbf{v} \cdot \nabla)\mathbf{w} = \sum_{i=1}^d v_i \frac{\partial \mathbf{w}}{\partial x_i}$ for all vector functions $\mathbf{v} = (v_1, \dots, v_d)$,
 85 $\mathbf{w} = (w_1, \dots, w_d)$.

86 The Navier-Stokes equations are well-suited to numerically simulate laminar
 87 flows for which the Reynolds number

$$\text{Re}_f = \frac{\rho U L}{\mu} \quad (2)$$

88 is not too high, U and L being a characteristic velocity and a characteristic
 89 length scale of the problem, respectively. For high Reynolds numbers turbulence
 90 effects become important and the Navier-Stokes equations need to be augmented
 91 with turbulence models, such as the RANS (Reynolds Averaged Navier-Stokes)
 92 ones. In our applications we will always place ourselves in the laminar case.

93 *2.2. Filtration through the porous domain*

94 Filtration through a saturated porous domain can be modeled by the Darcy
 95 law, which introduces an average fluid velocity on sample volumes of the porous
 96 medium sufficiently large with respect to the pore size.

97 The Darcy law is the simplest (linear) relation between the seepage velocity
 98 \mathbf{u}_p and the pressure p_p in the porous medium, and it states that

$$\mathbf{u}_p = -\frac{K}{\mu} \nabla p_p \quad \text{in } \Omega_p, \quad (3)$$

99 where μ is the dynamic viscosity coefficient already defined in (1), while K is
 100 the permeability coefficient. This law was originally obtained by Darcy with
 101 a famous experiment [18], and later rigorously derived from the Navier-Stokes
 102 equations by mathematical homogenization on structured porous grids (see,
 103 e.g., [50]). The permeability coefficient K can assume values ranging from
 104 $K = 10^{-5} m^2$ for very porous artificial materials to $K = 10^{-20} m^2$ for particular
 105 kind of soils or rocks. In case of a non-isotropic medium the scalar coefficient
 106 K is substituted by a permeability tensor \mathbf{K} .

107 As the seepage velocity increases, the transition towards a non-linear drag
 108 is quite smooth. In order to characterize the importance of the inertial effects,
 109 similarly to the Navier-Stokes equations, it is possible to define the Reynolds
 110 number associated to the pores

$$\text{Re}_p = \frac{\rho U \delta}{\mu}, \quad (4)$$

111 where δ is the characteristic pore size.

112 The Darcy law is reliable for values of $\text{Re}_p < 1$ (see, e.g., [4]), otherwise it
 113 is necessary to consider a more general model which can account also for the
 114 inertial effects, like the non-linear Forchheimer equation [25]:

$$\nabla p_p = -\frac{\mu}{K} \mathbf{u}_p - \frac{\rho C_F}{\sqrt{K}} |\mathbf{u}_p| \mathbf{u}_p \quad \text{in } \Omega_p, \quad (5)$$

115 where C_F is the inertial resistance coefficient (or tensor in the non-isotropic
 116 case). The transition between the Darcy and the Forchheimer regimes occurs
 117 in the range $1 < \text{Re}_p < 10$. More in general, non-linear correction terms of
 118 the form $|\mathbf{u}_p|^\alpha \mathbf{u}_p$ with $1 \leq \alpha \leq 2$ can be considered for Darcy's law. Detailed
 119 discussions about their physical interpretation can be found in [23, 43]. As the
 120 Darcy law, the Forchheimer equation can be derived by homogenization from
 121 the Navier-Stokes equations (see [15]).

122 The filtration model is fully determined considering the continuity equation:

$$\nabla \cdot \mathbf{u}_p = 0 \quad \text{in } \Omega_p. \quad (6)$$

123 The latter, combined with the Darcy equation (3), leads to the following elliptic
 124 equation involving only the pressure:

$$-\nabla \cdot \left(\frac{K}{\mu} \nabla p_p \right) = 0 \quad \text{in } \Omega_p. \quad (7)$$

125 If only (7) is solved in Ω_p , then the velocity can be recovered using the Darcy
 126 law (3).

127 *2.3. Coupling conditions across the interface*

128 To represent the filtration of the free fluid through the porous medium,
 129 we have to introduce suitable coupling conditions between the Navier-Stokes

130 and Darcy (or Forchheimer) equations across their common interface Γ . In
 131 particular, we consider the following three conditions.

132 1. Continuity of the normal component of the velocity:

$$\mathbf{u}_f \cdot \mathbf{n}_f = -\mathbf{u}_p \cdot \mathbf{n}_p \quad \text{on } \Gamma, \quad (8)$$

133 where \mathbf{n}_f and \mathbf{n}_p are the unit normal vectors external to $\partial\Omega_f$ and $\partial\Omega_p$,
 134 respectively (see Figure 1). Notice that $\mathbf{n}_f = -\mathbf{n}_p$ on Γ . Using Darcy law
 135 (3), equation (8) can be rewritten as

$$\mathbf{u}_f \cdot \mathbf{n}_f = \frac{K}{\mu} \frac{\partial p_p}{\partial n_p} \quad \text{on } \Gamma. \quad (9)$$

136 This condition is a consequence of the incompressibility of the fluid.

137 2. Continuity of the normal stresses across Γ (see, e.g., [36]):

$$p_f - \mu \frac{\partial \mathbf{u}_f}{\partial n_f} \cdot \mathbf{n}_f = p_p \quad \text{on } \Gamma. \quad (10)$$

138 Remark that pressures may be discontinuous across the interface.

139 3. Finally, in order to have a completely determined flow in the free-fluid
 140 region, we have to specify a further condition on the tangential component
 141 of the fluid velocity at the interface.

142 Beavers and Joseph [5] proposed an experimental condition stating that
 143 the difference between the slip velocity and the tangential seepage velocity
 144 at the interface is proportional to the shear rate therein:

$$-\left(\frac{\partial \mathbf{u}_f}{\partial n_f}\right)_\tau = \frac{\alpha_{BJ}}{\sqrt{K}} (\mathbf{u}_f - \mathbf{u}_p)_\tau \quad \text{on } \Gamma. \quad (11)$$

145 By $(\mathbf{v})_\tau$ we indicate the tangential component to the interface of the vector
 146 \mathbf{v} :

$$(\mathbf{v})_\tau = \mathbf{v} - \mathbf{v} \cdot \mathbf{n} \quad \text{on } \Gamma. \quad (12)$$

147 The constant α_{BJ} usually assumes values between 0.8 and 1.2 (see [5]).

148 Since the seepage velocity \mathbf{u}_p is far smaller than the fluid slip velocity \mathbf{u}_f
 149 at the interface, Saffman proposed to use the following simplified condition
 150 (the so-called Beavers-Joseph-Saffman condition) [49]:

$$-\left(\frac{\partial \mathbf{u}_f}{\partial n_f}\right)_\tau = \frac{\alpha_{BJ}}{\sqrt{K}} (\mathbf{u}_f)_\tau \quad \text{on } \Gamma. \quad (13)$$

151 This condition was later derived mathematically by homogenization by
152 Jäger and Mikelić [36, 37, 38].

153 The three coupling conditions described in this section have been extensively
154 studied and analyzed also in [20, 21, 40, 45, 48, 51].

155 **Remark 2.1.** *Notice that we have written the Navier-Stokes equations in time-*
156 *dependent form, while we consider steady models for the flow in the porous*
157 *medium. This can be justified by the fact that the velocity in the fluid domain*
158 *is generally much higher than the seepage velocity, so that the latter can be*
159 *treated as steady at least during small time intervals. If this assumption was*
160 *not satisfied, it would be possible to consider an unsteady model also in Ω_p as*
161 *studied for example in [12].*

162 2.4. Penalization method

163 The coupled model discussed in the above sections is quite complex to solve,
164 mainly because of the intrinsic difference in nature between the equations in the
165 subdomains Ω_f and Ω_p . For this reason, the so-called penalization approach
166 has been introduced to model the flow over porous media (see, e.g., [9, 34, 35]).
167 This method consists in considering a modified set of Navier-Stokes equations in
168 the whole domain including two penalization terms associated to the resistance
169 induced by the porous medium in the subregion Ω_p . These terms are related to
170 the linear Darcy and the non-linear Forchheimer equations (3) and (5).

171 More precisely, we consider the momentum equation:

$$\rho \left(\frac{\partial \mathbf{u}}{\partial t} + (\mathbf{u} \cdot \nabla) \mathbf{u} \right) - \mu \Delta \mathbf{u} + \nabla p + \left(\frac{\mu}{K} \mathbf{u} + \frac{\rho C_F}{\sqrt{K}} |\mathbf{u}| \mathbf{u} \right) \chi_{\Omega_p} = \mathbf{0} \quad \text{in } \Omega, \quad (14)$$

172 where the physical constants are the same already introduced in (1) and (5),
173 while $\chi_{\Omega_p} = 1$ in Ω_p and $\chi_{\Omega_p} = 0$ elsewhere, so that the last two terms vanish
174 in the fluid domain. The variable \mathbf{u} corresponds to the real velocity in Ω_f and
175 to the seepage velocity in Ω_p .

176 **Remark 2.2.** *Notice that this method can be enhanced to deal with inner solid*
177 *regions too, following the so-called “fictitious domain” approach proposed in [39]:*

178 the modified Navier-Stokes equations are solved in the whole domain, with very
 179 strong variations of the permeability coefficient. Indeed, it can be rigorously
 180 shown via homogenization techniques (see [1]) that the proposed approach is
 181 consistent with the modeling of both solid ($K \rightarrow 0$) and fluid ($K \rightarrow +\infty$) regions.

182 Concerning the physical meaning of (14), the diffusive contribution $-\mu\Delta\mathbf{u}$
 183 has been shown to be consistent with the modeling of highly porous materials,
 184 such as, for example, synthetic foams with porosity greater than 0.6, and some-
 185 times it is referred to as Brinkmann [8], or Brinkmann-Forchheimer equation
 186 [52], possibly with $\tilde{\mu} \neq \mu$. On the other hand, the non-linear convective term
 187 $(\mathbf{u} \cdot \nabla)\mathbf{u}$ has been criticized as an unsatisfactory way to include non-linear in-
 188 ertial effects, since, for example, it vanishes even for a steady incompressible
 189 unidirectional flow, regardless of the magnitude of the velocity \mathbf{u} .

190 However, since the penalization method is much easier to implement than the
 191 coupled approach of Sections 2.1-2.3, it is widely used in commercial softwares.
 192 Indeed, most of the commercial packages capable of simulating flows in domains
 193 partially occupied by porous media are based on this approach (see, e.g., [13,
 194 2, 24]). In these codes, the porous medium is usually characterized by two
 195 constants P_v and P_i called, respectively, *viscous* and *inertial resistance* which
 196 are different from zero only in the porous domain Ω_p . Then, the following
 197 penalized Navier-Stokes equations are solved:

$$\begin{aligned} \rho\left(\frac{\partial\mathbf{u}}{\partial t} + (\mathbf{u} \cdot \nabla)\mathbf{u}\right) - \mu\Delta\mathbf{u} + \nabla p + P_v\mathbf{u} + P_i|\mathbf{u}|\mathbf{u} &= \mathbf{0} && \text{in } \Omega, \\ \nabla \cdot \mathbf{u} &= 0 && \text{in } \Omega, \end{aligned} \quad (15)$$

198 where

$$P_v = \begin{cases} 0 & \text{in } \Omega_f \\ \mu/K & \text{in } \Omega_p, \end{cases} \quad \text{and} \quad P_i = \begin{cases} 0 & \text{in } \Omega_f \\ \rho C_F/\sqrt{K} & \text{in } \Omega_p. \end{cases} \quad (16)$$

199 2.5. Dimensionless formulations

200 To better compare the models that we have considered, we introduce their
 201 dimensionless forms. We define the following dimensionless variables:

$$\mathbf{x}' = \frac{\mathbf{x}}{L}, \quad t' = \frac{U}{L}t, \quad \mathbf{u}'_f = \frac{\mathbf{u}_f}{U}, \quad \mathbf{u}'_p = \frac{\mathbf{u}_p}{U}, \quad p'_f = \frac{p_f}{\rho U^2}, \quad p'_p = \frac{p_p}{\rho U^2}, \quad (17)$$

202 where L and U are respectively a characteristic length and velocity for the
 203 problem (we use the same for both the fluid and the porous medium).

204 By substituting (17) in (1) (recall that in our case $\mathbf{F} = \mathbf{0}$) we obtain the
 205 dimensionless formulation of the Navier-Stokes equations:

$$\begin{aligned} \frac{\partial \mathbf{u}'_f}{\partial t'} + (\mathbf{u}'_f \cdot \nabla) \mathbf{u}'_f - \frac{1}{\text{Re}_f} \Delta \mathbf{u}'_f + \nabla p'_f &= \mathbf{0} & \text{in } \Omega_f, \\ \nabla \cdot \mathbf{u}'_f &= 0 & \text{in } \Omega_f, \end{aligned} \quad (18)$$

206 where Re_f is the Reynolds number defined in (2).

207 The dimensionless form of the Darcy law (3) becomes

$$\mathbf{u}'_p = -\text{Gr}_n \nabla p'_p \quad \text{in } \Omega_p, \quad (19)$$

208 where the dimensionless group Gr_n is defined as

$$\text{Gr}_n = \frac{\rho K U}{\mu L}. \quad (20)$$

209 On the other hand, the dimensionless form of the Forchheimer equation (5)
 210 reads:

$$\mathbf{u}'_p + \text{Gr}_f |\mathbf{u}'_p| \mathbf{u}'_p = -\text{Gr}_n \nabla p'_p \quad \text{in } \Omega_p, \quad (21)$$

211 having denoted by Gr_f the dimensionless group

$$\text{Gr}_f = \frac{\rho C_F U \sqrt{K}}{\mu}. \quad (22)$$

212 The three coupling conditions (9), (10), (13) at the interface are make di-
 213 mensionless too, obtaining

$$\mathbf{u}'_f \cdot \mathbf{n}_f = \text{Gr}_n \frac{\partial p'_p}{\partial n'_p}, \quad (23)$$

$$p'_f - \frac{1}{\text{Re}_f} \frac{\partial \mathbf{u}'_f}{\partial n'_f} \cdot \mathbf{n}_f = p'_p, \quad (24)$$

$$-\left(\frac{\partial \mathbf{u}'_f}{\partial n'_f} \right)_\tau = \text{Gr}_c (\mathbf{u}'_f)_\tau, \quad (25)$$

214 where Gr_c is defined by

$$\text{Gr}_c = \frac{\alpha_{BJ} L}{\sqrt{K}}. \quad (26)$$

215 Finally, the dimensionless form of the penalized Navier-Stokes equations (15)
 216 becomes

$$\frac{\partial \mathbf{u}'}{\partial t'} + (\mathbf{u}' \cdot \nabla) \mathbf{u}' - \frac{1}{\text{Re}} \Delta \mathbf{u}' + \nabla p' + \text{Gr}_v \mathbf{u}' + \text{Gr}_i |\mathbf{u}'| \mathbf{u}' = \mathbf{0} \quad \text{in } \Omega, \quad (27)$$

217 with dimensionless groups

$$\text{Re} = \frac{\rho L U}{\mu}, \quad \text{Gr}_v = \frac{P_v L}{\rho U}, \quad \text{Gr}_i = \frac{P_i L}{\rho}. \quad (28)$$

218 In the following we will refer to the dimensionless formulations omitting the
 219 apices for simplicity of notation.

220 For the sake of clarity, let us summarize the models that we will consider in
 221 the next sections.

222 • *Navier-Stokes/Darcy (NSD) model:*

$$\begin{aligned} \frac{\partial \mathbf{u}_f}{\partial t} + (\mathbf{u}_f \cdot \nabla) \mathbf{u}_f - \frac{1}{\text{Re}_f} \Delta \mathbf{u}_f + \nabla p_f &= \mathbf{0} & \text{in } \Omega_f, \\ \nabla \cdot \mathbf{u}_f &= 0 & \text{in } \Omega_f, \\ -\nabla \cdot (\text{Gr}_n \nabla p_p) &= 0 & \text{in } \Omega_p, \\ \mathbf{u}_f \cdot \mathbf{n}_f &= \text{Gr}_n \frac{\partial p_p}{\partial n_p} & \text{on } \Gamma, \\ p_f - \frac{1}{\text{Re}_f} \frac{\partial \mathbf{u}_f}{\partial n_f} \cdot \mathbf{n}_f &= p_p & \text{on } \Gamma, \\ -\left(\frac{\partial \mathbf{u}_f}{\partial n_f} \right)_\tau &= \text{Gr}_c (\mathbf{u}_f)_\tau & \text{on } \Gamma. \end{aligned} \quad (29)$$

223 • *Navier-Stokes/Forchheimer (NSF) model:*

$$\begin{aligned} \frac{\partial \mathbf{u}_f}{\partial t} + (\mathbf{u}_f \cdot \nabla) \mathbf{u}_f - \frac{1}{\text{Re}_f} \Delta \mathbf{u}_f + \nabla p_f &= \mathbf{0} & \text{in } \Omega_f, \\ \nabla \cdot \mathbf{u}_f &= 0 & \text{in } \Omega_f, \\ \mathbf{u}_p + \text{Gr}_f |\mathbf{u}_p| \mathbf{u}_p - \text{Gr}_n \nabla p_p &= 0 & \text{in } \Omega_p, \\ \nabla \cdot \mathbf{u}_p &= 0 & \text{in } \Omega_p, \\ \mathbf{u}_f \cdot \mathbf{n}_f &= -\mathbf{u}_p \cdot \mathbf{n}_p & \text{on } \Gamma, \\ p_f - \frac{1}{\text{Re}_f} \frac{\partial \mathbf{u}_f}{\partial n_f} \cdot \mathbf{n}_f &= p_p & \text{on } \Gamma, \\ -\left(\frac{\partial \mathbf{u}_f}{\partial n_f} \right)_\tau &= \text{Gr}_c (\mathbf{u}_f)_\tau & \text{on } \Gamma. \end{aligned} \quad (30)$$

224 • *Penalization (PE) model:*

$$\begin{aligned} \frac{\partial \mathbf{u}}{\partial t} + (\mathbf{u} \cdot \nabla) \mathbf{u} - \frac{1}{\text{Re}} \Delta \mathbf{u} + \nabla p + \text{Gr}_v \mathbf{u} + \text{Gr}_i |\mathbf{u}| \mathbf{u} &= \mathbf{0} & \text{in } \Omega, \\ \nabla \cdot \mathbf{u} &= 0 & \text{in } \Omega. \end{aligned} \quad (31)$$

225 All the physical variables are dimensionless. Suitable boundary conditions
226 will be introduced in Section 2.6.

227 *2.6. Boundary conditions*

228 We set now the boundary conditions referring, for simplicity to a specific 2D
229 problem, but what we present can be extended to more general settings.

230 We consider the setting in Figure 2, in which a horizontal fluid flows upon
231 a saturated porous medium. The flow enters from the fluid inlet γ_1 and exits
232 at both the fluid and porous outlets γ_3 and δ_3 . All the other boundaries are
233 impermeable, with no-slip condition on γ_2 and with a slip condition on δ_1 and
234 δ_2 . As reference dimensionless parameters we consider L as the height of the
235 fluid channel and U as the maximal velocity at the inlet.

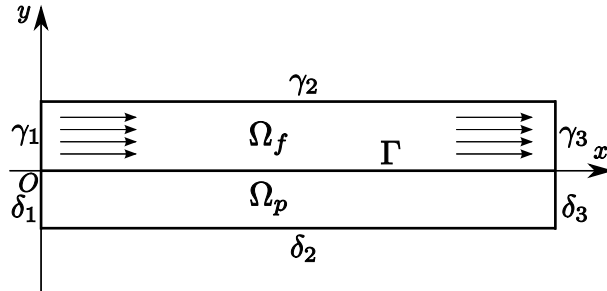


Figure 2: Scheme of the bidimensional sample problem.

236 More precisely, the boundary conditions that we use for the NSD model (29)

237 read:

$$\begin{aligned}
\mathbf{u}_f &= \mathbf{u}_{pois} && \text{on } \gamma_1, \\
\mathbf{u}_f &= \mathbf{0} && \text{on } \gamma_2, \\
p_f \mathbf{n}_f - \frac{1}{\text{Re}_f} \frac{\partial \mathbf{u}_f}{\partial n_f} &= \mathbf{0} && \text{on } \gamma_3, \\
\frac{\partial p_p}{\partial n_p} &= 0 && \text{on } \delta_1 \cup \delta_2, \\
p_p &= 0 && \text{on } \delta_3.
\end{aligned} \tag{32}$$

The function \mathbf{u}_{pois} is a given Poiseuille velocity profile on γ_1 . The same boundary conditions apply for the NSF problem (30) with (32)₄ replaced by

$$\mathbf{u}_p \cdot \mathbf{n}_p = 0 \quad \text{on } \delta_1 \cup \delta_2.$$

238 For the PE problem (31), we have to impose a slightly different set of bound-
239 ary conditions:

$$\begin{aligned}
\mathbf{u} &= \mathbf{u}_{pois} && \text{on } \gamma_1, \\
\mathbf{u} &= \mathbf{0} && \text{on } \gamma_2, \\
p \mathbf{n} - \frac{1}{\text{Re}} \frac{\partial \mathbf{u}}{\partial n} &= \mathbf{0} && \text{on } \gamma_3, \\
\mathbf{u} \cdot \mathbf{n} &= 0 && \text{on } \delta_1 \cup \delta_2, \\
\left(\frac{\partial \mathbf{u}}{\partial n} \right)_\tau &= 0 && \text{on } \delta_1 \cup \delta_2, \\
p \mathbf{n} - \frac{1}{\text{Re}} \frac{\partial \mathbf{u}}{\partial n} &= \mathbf{0} && \text{on } \delta_3.
\end{aligned} \tag{33}$$

240 Notice that condition (32)₅ has been replaced by (33)₆ since in the latter case
241 the stress on δ_3 is not given by the sole pressure, but by the whole Cauchy
242 stress tensor. Moreover, condition (32)₄ has been changed into (33)₄ and (33)₅.
243 Indeed, thanks to Darcy's law, (32)₄ corresponds to the null normal velocity
244 condition (33)₄, while (33)₅ has been introduced to ensure the well-posedness
245 of the problem.

246 As initial condition for all models we assume the velocity in the fluid region
247 Ω_f to be equal to the Poiseuille flow profile at the initial time, i.e., $\mathbf{u}_f(t=0) =$
248 \mathbf{u}_{pois} in Ω_f . On the other hand, we assume that at the initial time there is no
249 flow in the porous medium, and that at the beginning of the simulation a rigid
250 impermeable device separating the two domains is suddenly removed, allowing
251 the penetration of the fluid in the porous bed.

252 **3. Numerical approximation and solution algorithms**

253 In this section we address the finite element approximation of the coupled
 254 problems considered in Sections 2.5-2.6 and we propose an iterative solution
 255 method based on a domain decomposition approach.

256 *3.1. Space discretization*

257 We consider a regular triangulation \mathcal{T}_h of the domain $\bar{\Omega}_f \cup \bar{\Omega}_p$, depending
 258 on a positive parameter $h > 0$, made up of triangles T . We assume that the
 259 triangulations \mathcal{T}_{fh} and \mathcal{T}_{ph} induced on the subdomains Ω_f and Ω_p are compat-
 260 ible on Γ , that is they share the same edges therein. Finally, we suppose the
 261 triangulation induced on Γ to be quasi-uniform (see, e.g., [46]). An example of
 262 regular compatible triangulation is shown in Figure 3.

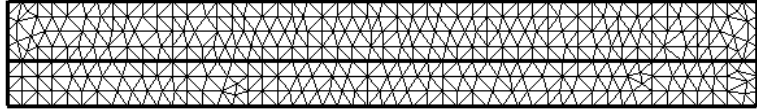


Figure 3: Example of regular compatible computational mesh.

Several choices of finite element spaces can be made. If we indicate by \mathbf{W}_h and Q_h the finite element spaces which approximate the velocity and pressure fields, respectively, for the Navier-Stokes problem or for the penalization model, there must exist a positive constant $\beta^* > 0$, independent of h , such that the classical inf-sup condition is satisfied, i.e., $\forall q_h \in Q_h, \exists \mathbf{v}_h \in \mathbf{W}_h, \mathbf{v}_h \neq \mathbf{0}$, such that

$$\int_{\mathcal{D}} q_h \nabla \cdot \mathbf{v}_h \geq \beta^* \|\mathbf{v}_h\|_{H^1(\mathcal{D})} \|q_h\|_{L^2(\mathcal{D})},$$

263 where $\mathcal{D} = \Omega_f$ for (29) and (30) and $\mathcal{D} = \Omega$ for (31).

264 Several families of finite element spaces satisfying the inf-sup condition are
 265 provided in [7]. In the following, for the sake of exposition, we will make the
 266 special choice of piecewise quadratic elements for the velocity and piecewise
 267 linear for the pressure.

268 More precisely, we start by defining the following discrete spaces for the NSD
 269 problem:

$$\begin{aligned}
 \mathbf{X}_{fh} &= \{\mathbf{v}_h \in \mathcal{C}^0(\overline{\Omega}_f) : \mathbf{v}_{h|T} \in [\mathbb{P}_2(T)]^2 \forall T \in \mathcal{T}_{fh}\}, \\
 \mathbf{V}_{fh} &= \{\mathbf{v}_h \in \mathbf{X}_{fh} : \mathbf{v}_h = \mathbf{0} \text{ on } \gamma_1 \cup \gamma_2\}, \\
 Q_{fh} &= \{q_h \in \mathcal{C}^0(\overline{\Omega}_f) : q_{h|T} \in \mathbb{P}_1(T) \forall T \in \mathcal{T}_{fh}\}, \\
 W_{ph} &= \{q_h \in \mathcal{C}^0(\overline{\Omega}_p) : q_{h|T} \in \mathbb{P}_2(T) \forall T \in \mathcal{T}_{ph}, q_h = 0 \text{ on } \delta_3\}.
 \end{aligned}$$

270 Then, the Galerkin approximation of the coupled NSD problem (29) reads: find
 271 $\mathbf{u}_{fh}(t) \in \mathbf{X}_{fh}$, $p_{fh}(t) \in Q_{fh}$, $p_{ph} \in W_{ph}$ such that

$$\begin{aligned}
 & \int_{\Omega_f} \frac{\partial \mathbf{u}_{fh}}{\partial t} \cdot \mathbf{v}_{fh} + \int_{\Omega_f} \left((\mathbf{u}_{fh} \cdot \nabla) \mathbf{u}_{fh} \right) \cdot \mathbf{v}_{fh} + \int_{\Omega_f} \frac{1}{\text{Re}_f} \nabla \mathbf{u}_{fh} \cdot \nabla \mathbf{v}_{fh} \\
 & \quad - \int_{\Omega_f} p_{fh} \nabla \cdot \mathbf{v}_{fh} + \int_{\Gamma} p_{ph} \mathbf{v}_{fh} \cdot \mathbf{n}_f \\
 & \quad + \int_{\Gamma} \frac{\text{Gr}_c}{\text{Re}_f} (\mathbf{u}_{fh})_{\tau} \cdot (\mathbf{v}_{fh})_{\tau} = 0 \quad \forall \mathbf{v}_{fh} \in \mathbf{V}_{fh}, \\
 & \int_{\Omega_f} q_{fh} \nabla \cdot \mathbf{u}_{fh} = 0 \quad \forall q_{fh} \in Q_{fh}, \\
 & \int_{\Omega_p} \text{Gr}_n \nabla p_{ph} \cdot \nabla q_{ph} - \int_{\Gamma} \mathbf{u}_{fh} \cdot \mathbf{n}_f q_{ph} = 0 \quad \forall q_{ph} \in W_{ph},
 \end{aligned} \tag{34}$$

272 with $\mathbf{u}_{fh}(t) = \mathbf{u}_{pois}^h$ on γ_1 , $\mathbf{u}_{fh}(t) = \mathbf{0}$ on γ_2 and $\mathbf{u}_{fh}(0) = \mathbf{u}_{pois}^h$ in Ω_f . \mathbf{u}_{pois}^h is
 273 a suitable approximation of \mathbf{u}_{pois} in the finite element space \mathbf{X}_{fh} .

274 (The mathematical analysis of the time-dependent NSD problem has been re-
 275 cently carried out in [14].)

276 In the case of the NSF problem (30), we cannot eliminate the unknown
 277 velocity \mathbf{u}_p in Ω_p as done for the Darcy equation. Thus, to write the Galerkin
 278 approximation of (30) we should consider a suitable family of inf-sup stable
 279 finite element spaces also in the porous domain. Moreover, we should introduce
 280 Lagrange multipliers to impose the continuity condition (30)₅, following the
 281 approach used in [40] to deal with the velocity-pressure formulation of the Darcy
 282 problem. However, in our applications we will not use such mixed formulation
 283 for the Forchheimer equation, but we will solve only for p_p in Ω_p , as explained in
 284 Section 3.3. Thus, we do not discuss here the mixed finite element formulation
 285 and we refer the reader to [28, 32, 44].

286 In analogous way, we can define the following finite element spaces for the
 287 PE approach:

$$\begin{aligned}\mathbf{X}_h &= \{\mathbf{v}_h \in \mathcal{C}^0(\overline{\Omega}) : \mathbf{v}_h|_T \in [\mathbb{P}_2(T)]^2 \forall T \in \mathcal{T}_h\}, \\ \mathbf{V}_h &= \{\mathbf{v}_h \in \mathbf{X}_h : \mathbf{v}_h = \mathbf{0} \text{ on } \gamma_1 \cup \gamma_2 \text{ and } \mathbf{v}_h \cdot \mathbf{n} = 0 \text{ on } \delta_1 \cup \delta_2\}, \\ Q_h &= \{q_h \in \mathcal{C}^0(\overline{\Omega}) : q_h|_T \in \mathbb{P}_1(T) \forall T \in \mathcal{T}_h\}.\end{aligned}$$

288 The Galerkin approximation of (31) reads: find $\mathbf{u}_h(t) \in \mathbf{X}_h$, $p_h \in Q_h$ such that

$$\begin{aligned}\int_{\Omega} \frac{\partial \mathbf{u}_h}{\partial t} \cdot \mathbf{v}_h + \int_{\Omega} \left((\mathbf{u}_h \cdot \nabla) \mathbf{u}_h \right) \cdot \mathbf{v}_h + \int_{\Omega} \frac{1}{\text{Re}} \nabla \mathbf{u}_h \cdot \nabla \mathbf{v}_h - \int_{\Omega} p_h \nabla \cdot \mathbf{v}_h \\ + \int_{\Omega} \text{Gr}_v \mathbf{u}_h \cdot \mathbf{v}_h + \int_{\Omega} \text{Gr}_i |\mathbf{u}_h| \mathbf{u}_h \cdot \mathbf{v}_h = 0 \quad \forall \mathbf{v}_h \in \mathbf{V}_h, \\ \int_{\Omega} q_h \nabla \cdot \mathbf{u}_h = 0 \quad \forall q_h \in Q_h,\end{aligned} \quad (35)$$

289 with $\mathbf{u}_h(t) = \mathbf{u}_{pois}^h$ on γ_1 , $\mathbf{u}_h(t) = \mathbf{0}$ on γ_2 , $\mathbf{u}_h(0) = \mathbf{u}_{pois}^h$ in Ω_f and $\mathbf{u}_h(0) = \mathbf{0}$
 290 in Ω_p . \mathbf{u}_{pois}^h is a suitable approximation of \mathbf{u}_{pois} in the finite element space \mathbf{X}_h .

291 3.2. Time discretization

292 To carry out the time discretization we keep in mind our main application:
 293 the simulation of the stationary air flow over the porous comfort layer inside a
 294 motorbike helmet. Then, since we are interested in the steady state solution,
 295 we adopt a first-order implicit Euler scheme with a semi-implicit treatment of
 296 the nonlinear convective term of the Navier-Stokes equations.

297 We subdivide the time interval considering a fixed time step Δt : $0 = t^0 <$
 298 $t^1 < \dots < t^n < t^{n+1} < \dots$, $t^{n+1} - t^n = \Delta t$, $\forall n \geq 0$, and we denote by the upper
 299 index n a quantity computed at the time step t^n .

300 Thus, the discretization in time and space of the coupled NSD problem (34)

301 becomes: for $n \geq 0$, find $\mathbf{u}_{fh}^{n+1} \in \mathbf{X}_{fh}$, $p_{fh}^{n+1} \in Q_{fh}$, $p_{ph} \in W_{ph}$ such that

$$\begin{aligned}
& \frac{1}{\Delta t} \int_{\Omega_f} \mathbf{u}_{fh}^{n+1} \cdot \mathbf{v}_{fh} + \int_{\Omega_f} \left((\mathbf{u}_{fh}^n \cdot \nabla) \mathbf{u}_{fh}^{n+1} \right) \cdot \mathbf{v}_{fh} + \int_{\Omega_f} \frac{1}{\text{Re}_f} \nabla \mathbf{u}_{fh}^{n+1} \cdot \nabla \mathbf{v}_{fh} \\
& \quad - \int_{\Omega_f} p_{fh}^{n+1} \nabla \cdot \mathbf{v}_{fh} + \int_{\Gamma} p_{ph} \mathbf{v}_{fh} \cdot \mathbf{n}_f \\
& \quad + \int_{\Gamma} \frac{\text{Gr}_c}{\text{Re}_f} (\mathbf{u}_{fh}^{n+1})_{\tau} \cdot (\mathbf{v}_{fh})_{\tau} = \frac{1}{\Delta t} \int_{\Omega_f} \mathbf{u}_{fh}^n \cdot \mathbf{v}_{fh} \quad \forall \mathbf{v}_{fh} \in \mathbf{V}_{fh}, \\
& \int_{\Omega_f} q_{fh} \nabla \cdot \mathbf{u}_{fh}^{n+1} = 0 \quad \forall q_{fh} \in Q_{fh}, \\
& \int_{\Omega_p} \text{Gr}_n \nabla p_{ph} \cdot \nabla q_{ph} - \int_{\Gamma} \mathbf{u}_{fh}^{n+1} \cdot \mathbf{n}_f q_{ph} = 0 \quad \forall q_{ph} \in W_{ph},
\end{aligned} \tag{36}$$

302 with $\mathbf{u}_{fh}^0 = \mathbf{u}_{pois}^h$ in Ω_f and $\mathbf{u}_{fh}^n = \mathbf{u}_{pois}^h$ on γ_1 , $\mathbf{u}_{fh}^n = \mathbf{0}$ on γ_2 for all $n \geq 0$.

303 On the other hand, for the PE model (35) we consider also a semi-implicit
304 treatment of the nonlinear Forchheimer correction. Thus, its space-time dis-
305 cretization becomes: find $\mathbf{u}_h^{n+1} \in \mathbf{X}_h$, $p_h^{n+1} \in Q_h$ such that

$$\begin{aligned}
& \frac{1}{\Delta t} \int_{\Omega} \mathbf{u}_h^{n+1} \cdot \mathbf{v}_h + \int_{\Omega} \left((\mathbf{u}_h^n \cdot \nabla) \mathbf{u}_h^{n+1} \right) \cdot \mathbf{v}_h + \int_{\Omega} \frac{1}{\text{Re}} \nabla \mathbf{u}_h^{n+1} \cdot \nabla \mathbf{v}_h \\
& \quad - \int_{\Omega} p_h^{n+1} \nabla \cdot \mathbf{v}_h + \int_{\Omega} \text{Gr}_v \mathbf{u}_h^{n+1} \cdot \mathbf{v}_h + \int_{\Omega} \text{Gr}_i |\mathbf{u}_h^n| \mathbf{u}_h^{n+1} \cdot \mathbf{v}_h \\
& \quad = \frac{1}{\Delta t} \int_{\Omega} \mathbf{u}_h^n \cdot \mathbf{v}_h \quad \forall \mathbf{v}_h \in \mathbf{V}_h, \\
& \int_{\Omega} q_h \nabla \cdot \mathbf{u}_h^{n+1} = 0 \quad \forall q_h \in Q_h,
\end{aligned} \tag{37}$$

306 with $\mathbf{u}_h^0 = \mathbf{u}_{pois}^h$ in Ω_f , $\mathbf{u}_h^0 = \mathbf{0}$ in Ω_p , $\mathbf{u}_h^n = \mathbf{u}_{pois}^h$ on γ_1 , $\mathbf{u}_h^n = \mathbf{0}$ on γ_2 for all
307 $n \geq 0$.

308 3.3. An iterative algorithm

309 To solve the coupled problem (36) we would like to set up an iterative method
310 requiring the alternate solution of the Navier-Stokes equations in Ω_f and of
311 the Darcy equation in Ω_p . To this aim, we consider a domain decomposition
312 approach similar to those studied in [19, 21].

313 Since for our applications we are interested in computing the steady state
314 solution, after discretizing in time we do not perform sub-iterations at each time
315 step, but we adopt the following scheme.

316 Let φ_h^0 and ψ_h^0 be suitable approximations at the initial time of the pressure
 317 p_{ph}^0 and of the normal velocity $\mathbf{u}_{fh}^0 \cdot \mathbf{n}_f$ on Γ , respectively. Moreover, let $0 \leq$
 318 $\alpha, \beta \leq 1$ be two relaxation parameters. Then, for $n \geq 0$

319 1. find $\mathbf{u}_{fh}^{n+1} \in \mathbf{X}_{fh}, p_{fh}^{n+1} \in Q_{fh}$ such that

$$\begin{aligned}
 & \frac{1}{\Delta t} \int_{\Omega_f} \mathbf{u}_{fh}^{n+1} \cdot \mathbf{v}_{fh} + \int_{\Omega_f} \left((\mathbf{u}_{fh}^n \cdot \nabla) \mathbf{u}_{fh}^{n+1} \right) \cdot \mathbf{v}_{fh} \\
 & + \int_{\Omega_f} \frac{1}{\text{Re}_f} \nabla \mathbf{u}_{fh}^{n+1} \cdot \nabla \mathbf{v}_{fh} - \int_{\Omega_f} p_{fh}^{n+1} \nabla \cdot \mathbf{v}_{fh} + \int_{\Gamma} \varphi_h^n \mathbf{v}_{fh} \cdot \mathbf{n}_f \\
 & + \int_{\Gamma} \frac{\text{Gr}_c}{\text{Re}_f} (\mathbf{u}_{fh}^{n+1})_{\tau} \cdot (\mathbf{v}_{fh})_{\tau} = \frac{1}{\Delta t} \int_{\Omega_f} \mathbf{u}_{fh}^n \cdot \mathbf{v}_{fh} \quad \forall \mathbf{v}_{fh} \in \mathbf{V}_{fh}, \\
 & \int_{\Omega_f} q_{fh} \nabla \cdot \mathbf{u}_{fh}^{n+1} = 0 \quad \forall q_{fh} \in Q_{fh}.
 \end{aligned} \tag{38}$$

320 2. Update the normal velocity of the fluid across Γ :

$$\psi_h^{n+1} = (1 - \beta) \psi_h^n + \beta \mathbf{u}_{fh}^{n+1} \cdot \mathbf{n}_f \quad \text{on } \Gamma. \tag{39}$$

321 3. Find $p_{ph}^{n+1} \in W_{ph}$ such that

$$\int_{\Omega_p} \text{Gr}_n \nabla p_{ph}^{n+1} \cdot \nabla q_{ph} - \int_{\Gamma} \psi_h^{n+1} q_{ph} = 0 \quad \forall q_{ph} \in W_{ph}. \tag{40}$$

322 4. Compute the new pressure across Γ :

$$\varphi_h^{n+1} = (1 - \alpha) \varphi_h^n + \alpha p_{ph}^{n+1} \quad \text{on } \Gamma. \tag{41}$$

323 5. Increment n and go back to step 1.

324 This algorithm requires at each step to solve separately and in a sequential
 325 fashion the Navier-Stokes equations in Ω_f and the Darcy equations in Ω_p . Its
 326 structure resembles the classical Dirichlet-Neumann method in domain decom-
 327 position (see, e.g., [47]). However, notice that here, due to the characteristics of
 328 the problems at hand, the conditions imposed on the interface are of Neumann
 329 type for both sub-problems.

330 This approach allows us to easily replace the Darcy model by the Forch-
 331 heimer equation solving the latter only for p_{ph} at each iteration. Indeed, adopt-
 332 ing a semi-implicit treatment of the nonlinear term of the Forchheimer equation,

333 instead of (40) we consider the problem: find $p_{ph}^{n+1} \in W_{ph}$ such that

$$\int_{\Omega_p} \frac{\text{Gr}_n}{1 + \text{Gr}_f |\mathbf{u}_{ph}^n|} \nabla p_{ph}^{n+1} \cdot \nabla q_{ph} - \int_{\Gamma} \psi_h^{n+1} q_{ph} = 0 \quad \forall q_{ph} \in W_{ph}. \quad (42)$$

334 The velocity in Ω_p at time t^{n+1} can then be recovered by:

$$\mathbf{u}_p^{n+1} = -\frac{\text{Gr}_n}{1 + \text{Gr}_f |\mathbf{u}_p^n|} \nabla p_p^{n+1} \quad \text{in } \Omega_p. \quad (43)$$

335 4. Numerical comparison between the different models in a 2D test 336 case

337 In this section we present some numerical results on a 2D test case using the
338 three models studied in the previous sections.

339 We consider a 2D computational domain as shown in Figure 2 to represent an
340 air flow in a channel over a slightly porous tissue. We set $\rho = 1.184 \text{ kg/m}^3$,
341 $\mu = 1.855 \cdot 10^{-5} \text{ Pa s}$, $K = 3.71 \cdot 10^{-7} \text{ m}^2$, $\alpha_{BJ} = 1.0$, $C_F = 0.5$. Referring to
342 Figure 2, our domain has length of 50 mm in the x -direction, height of 4 mm
343 in the fluid domain and of 3 mm in the porous region.

344 As reference characteristic quantities we consider $L = 10^{-3} \text{ m}$ and $U = 10^{-1} \text{ m/s}$.

345 Thus, the dimensionless parameters characterizing the models NSD, NSF and
346 PE are: $\text{Re}_f = 6.38$, $\text{Gr}_n = 2.37$, $\text{Gr}_f = 1.94$, $\text{Gr}_c = 1.64$, $\text{Gr}_v = 0.42$ and
347 $\text{Gr}_i = 0.82$. (The dimensionless domain has dimension of 50 unit lengths in the
348 x -direction and height of 4 and 3 unit lengths in the fluid and in the porous
349 medium regions, respectively.) Notice that in our case it is difficult to quantify
350 Re_p in (4) as the pore size δ is unknown. Boundary conditions are specified
351 as in Section 2.6 and the Poiseuille velocity profile on the inlet boundary γ_1 is
352 $\mathbf{u}_{pois} = (y(4 - y), 0)$.

353 The numerical implementation is carried out in the finite element package
354 freeFEM++ [33], using the multi-frontal algorithms of UMFPACK for solving
355 the local linear systems. The computational grids are uniform, unstructured,
356 conforming on Γ and they are characterized by the adimensional grid parameter
357 $h = 1/N$, N being the number of partitions of each unit length. $\mathbb{P}_2 - \mathbb{P}_1$ finite
358 elements have been used for the spatial discretization.

359 We consider at first the NSF model with the iterative algorithm of Section 3.3.
 360 The NSF model permits to characterize explicitly Γ and to deal with larger
 361 Reynolds numbers Re_p in the porous media domain than if the Darcy model is
 362 adopted (see [4, 42]).

363 The finite element solution of the NSF problem at the steady state on a
 364 computational mesh with $N = 3$ corresponding to $h = 1/3$ and to about 6500
 365 elements is shown in Figure 4. We can see that the flow suddenly enters the
 366 porous medium creating a little recirculation region and then it stabilizes in an
 367 almost horizontal flow.

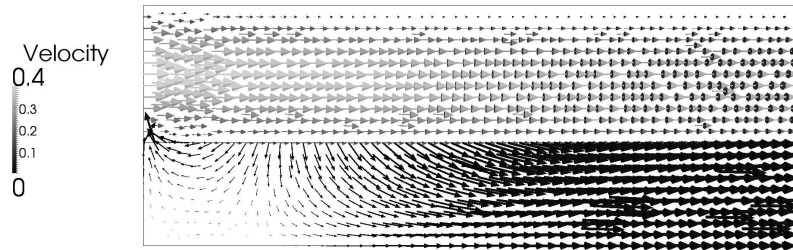


Figure 4: Vector plot of the steady-state flow field (only the first 25 length units in the x -direction are visualized) computed with the NSF model.

368 The normal component of the velocity through the interface is plotted in
 369 Figure 5(a), which clearly highlights that the major filtration occurs during the
 370 first 15-20 length units. The velocity profile at the outlet (i.e., at 50 length units
 371 in the x direction) represented in Figure 5(b) shows that the fluid velocity close
 372 to the interface is higher than the seepage velocity in the porous medium.

The flow is conserved in the computational domain. Indeed, if we compute the flux on the boundaries:

$$\mathcal{F}_\gamma = \int_{\gamma_1 \cup \gamma_3 \cup \delta_3} \mathbf{u} \cdot \mathbf{n},$$

373 with obvious choice of notation we have $\mathcal{F}_{\gamma_1} = -10.667$, $\mathcal{F}_{\gamma_3} = 9.285$, $\mathcal{F}_{\delta_3} =$
 374 $\mathcal{F}_\Gamma = 1.382$, so that $\mathcal{F}_\gamma = 0$.

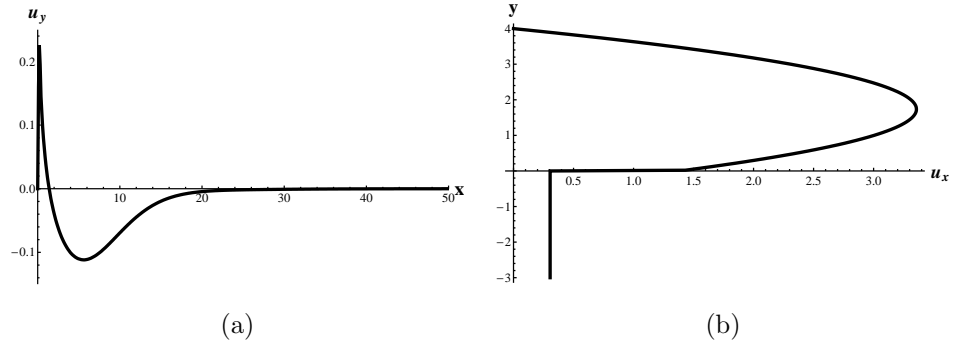


Figure 5: NSF model: normal velocity through the interface computed with respect to the y -direction (a) and velocity profile at the outlet (b) (i.e., at 50 length units in the x direction).

375 The velocity profile at the outlet can be also evaluated analytically for the
 376 NSF coupled problem under the assumption of a fully horizontal flow, that is
 377 placing oneself at infinite distance from the inlet. The velocity field in Ω_f be-
 378 comes $\mathbf{u}_f = (u(y), 0)$ where $u(y)$ is the solution of the boundary value problem:

$$-\frac{1}{Re_f} \frac{d^2 u}{dy^2} + \delta p = 0 \quad 0 \leq y \leq 4, \quad (44)$$

379 with the Dirichlet boundary condition on the top boundary:

$$u(4) = 0, \quad (45)$$

380 and with the Robin boundary condition at the contact interface with the porous
 381 medium:

$$u'(0) = Gr_c u(0). \quad (46)$$

382 Here, δp represents the constant value of the pressure drop along the x -direction.

383 On the other hand, the (constant) horizontal seepage velocity in the porous
 384 medium becomes $\mathbf{u}_p = (0, v)$ where v is the solution of the Forchheimer equation
 385 for the limit horizontal flow:

$$v + Gr_f v^2 + Gr_n \delta p = 0. \quad (47)$$

386 Moreover, we have to impose the flow conservation between the inlet and outlet
 387 boundaries:

$$\int_0^4 u_{pois}(y) dy = \int_0^4 u(y) dy + \int_{-3}^0 v dy, \quad (48)$$

388 u_{pois} being the x -component of \mathbf{u}_{pois} .

389 The solution of (44)-(48) is

$$u(y) = -\frac{D_1 \text{Re}_f}{2^{14} A_2 B_3 \text{Gr}_f} (y-4)(y+4+4\text{Gr}_c y), \quad (49)$$

$$v = \frac{1}{2\text{Gr}_f} \left(\sqrt{1 + \frac{D_1 \text{Gr}_n}{2^{11} B_3}} - 1 \right), \quad (50)$$

390 where $A_1 = 1 + \text{Gr}_c$, $A_2 = 1 + 4\text{Gr}_c$, $A_3 = 9 + 64\text{Gr}_f$, $B_1 = 64A_1 A_2 A_3 \text{Re}_f$,
 391 $B_2 = 81A_2^2 \text{Gr}_n$, $B_3 = A_1^2 \text{Re}_f^2$, $C_1 = A_2(2B_1 \text{Gr}_n + B_2 \text{Gr}_n + 2^{12} B_3)^{1/2}$, $D_1 =$
 392 $-9C_1 + B_1 + B_2$.

In the case that we are considering, we have

$$u(y) = 1.38426 + 2.27264y - 0.654677y^2 \quad \text{and} \quad v = 0.304974.$$

393 The computed and the analytical profiles are compared in Figure 6: as soon as
 394 the flow becomes parallel, which occurs near the outlet of the domain (i.e., at
 395 50 length units in the x direction), the analytical solution coincides with the
 396 numerical one. The numerical solution has been computed setting $N = 3$.

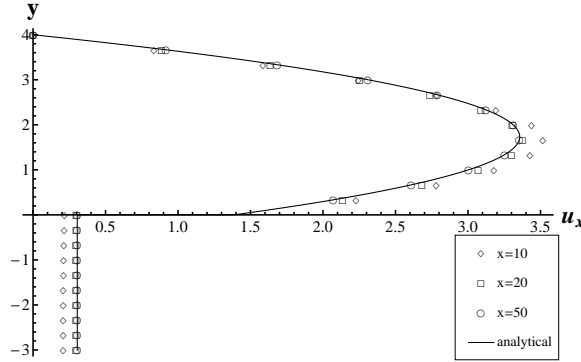


Figure 6: Comparison between the analytical solution (solid line) and the numerical results obtained with the NSF model on different sections along the x -direction (dots), for the x component of the velocity.

397 The effect of the Forchheimer coefficient C_F on the flow is illustrated in
 398 Figure 7, where we can see that the behavior of the flow in the recirculation

399 zone near the inlet is modified as well as the velocity profile at outlet. Moreover,
 400 from the physical viewpoint, we remark that as the Forchheimer coefficient raises
 401 from 0.0 to 0.5 (its range of variability) the flux filtrating into the porous medium
 402 decreases (see Figure 7(c)).

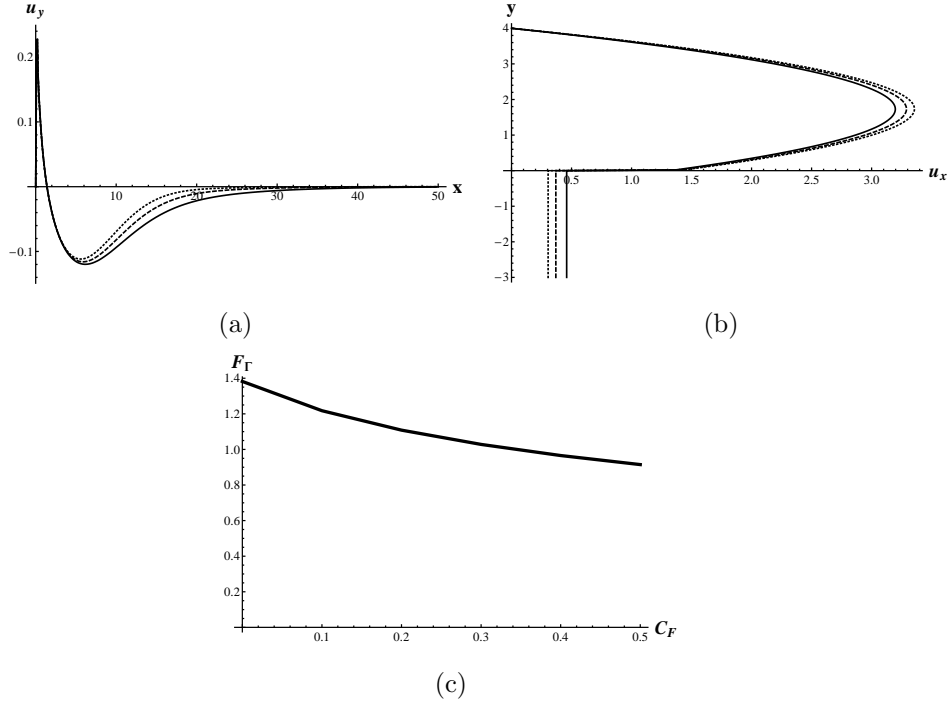


Figure 7: NSF model: (a) normal component of the velocity across the interface and (b) velocity profile at outlet for values of C_F of 0.0 (solid line), 0.2 (dashed line) and 0.5 (dotted line). (c) Flux entering the porous domain as a function of C_F .

403 Let us consider now the NSD model. With the same settings used for the
 404 NSF model, we compute the solution of the NSD problem for different values
 405 of the permeability K .

406 Figure 8 shows the computed normal velocities and outflow profiles for in-
 407 creasing values of K . As expected, as K grows, more and more flow enters the
 408 porous medium (see Figure 8(c)).

409 Moreover, for both the NSD and the NSF models, notice that for high values

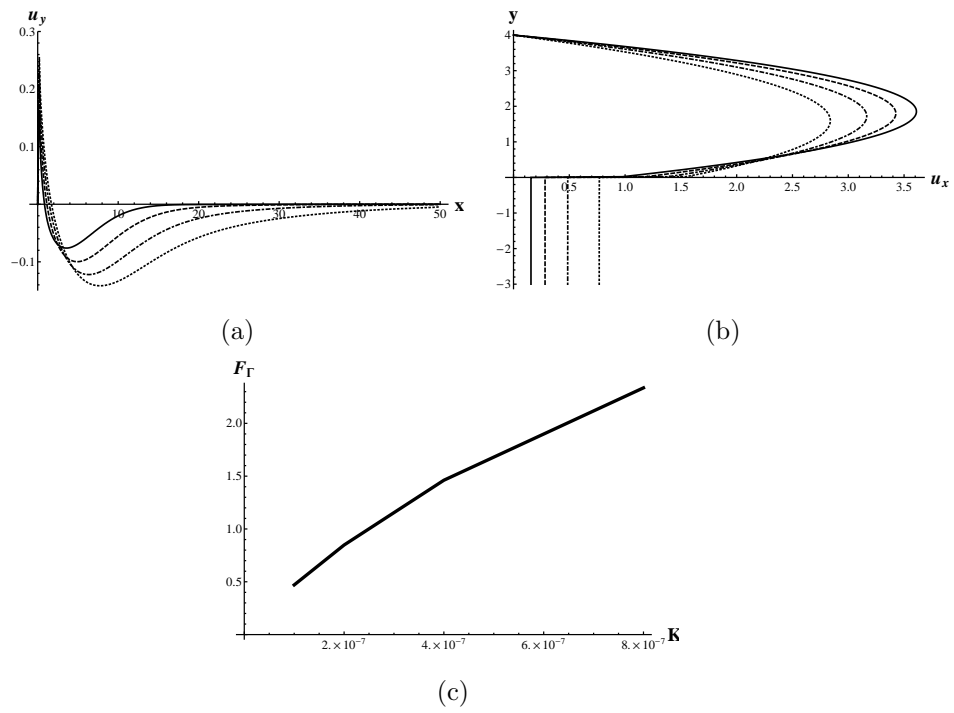


Figure 8: NSD model: (a) normal component of the velocity across the interface and (b) velocity profile at outlet for values of K equal to 10^{-7} (solid line), $2 \cdot 10^{-7}$ (dashed line), $4 \cdot 10^{-7}$ (dot-dashed line) and $8 \cdot 10^{-7}$ (dotted line). (c) Flux entering the porous domain as a function of K .

410 of the permeability the gap between the tangential component of the velocity of
 411 the fluid and the seepage velocity across the interface Γ reduces. Thus, Saffman's
 412 assumption $\mathbf{u}_p \ll \mathbf{u}_f$ on the interface is no more satisfied, and for large K the
 413 original Beavers and Joseph condition (11) cannot be replaced by (13). The
 414 difference between the two conditions can be directly seen on the computed
 415 velocity profile at the outlet (see Figure 9).

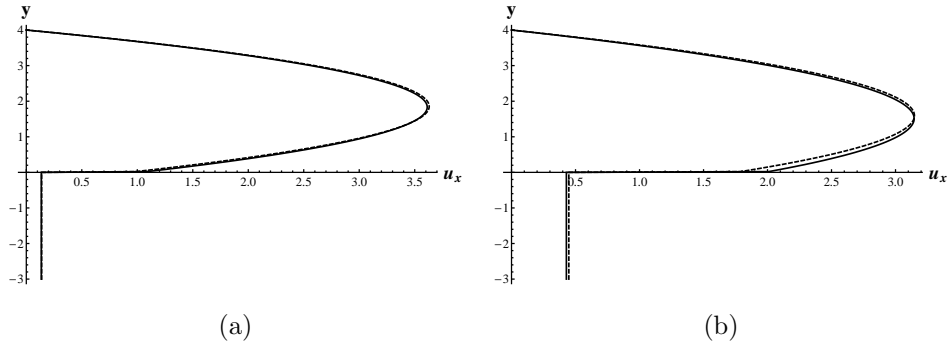


Figure 9: NSF model ($C_F = 0.5$): comparison between the velocity profile at outlet obtained using the Beavers-Joseph interface condition (solid line) and Beavers-Joseph-Saffman one (dashed line), for a small value of the permeability $K = 10^{-7} m^2$ (a) and a high one $K = 10^{-6} m^2$ (b).

416 The values of K used for the simulations reported in Figures 7(a)-(b) and
 417 8(a)-(b) are chosen to represent a porous medium with high permeability. In
 418 correspondence to such values, which are of interest for our target application
 419 (see Section 5), we can appreciate the difference between the results computed
 420 with two models NSD and NSF.

421 If the value of the permeability becomes smaller, the results computed with
 422 those two models cannot be distinguished as we can see in Figure 10, where we
 423 compare the velocities and fluxes obtained for values of K from 10^{-7} to 10^{-10}
 424 m^2 . In such cases, it seems not worth using the nonlinear Forchheimer model
 425 instead of the Darcy one.

426 We compare now NSD, NSF and PE. As expected, the PE model shows a
 427 very smooth transition of the velocity field from Ω_f to the porous medium, in

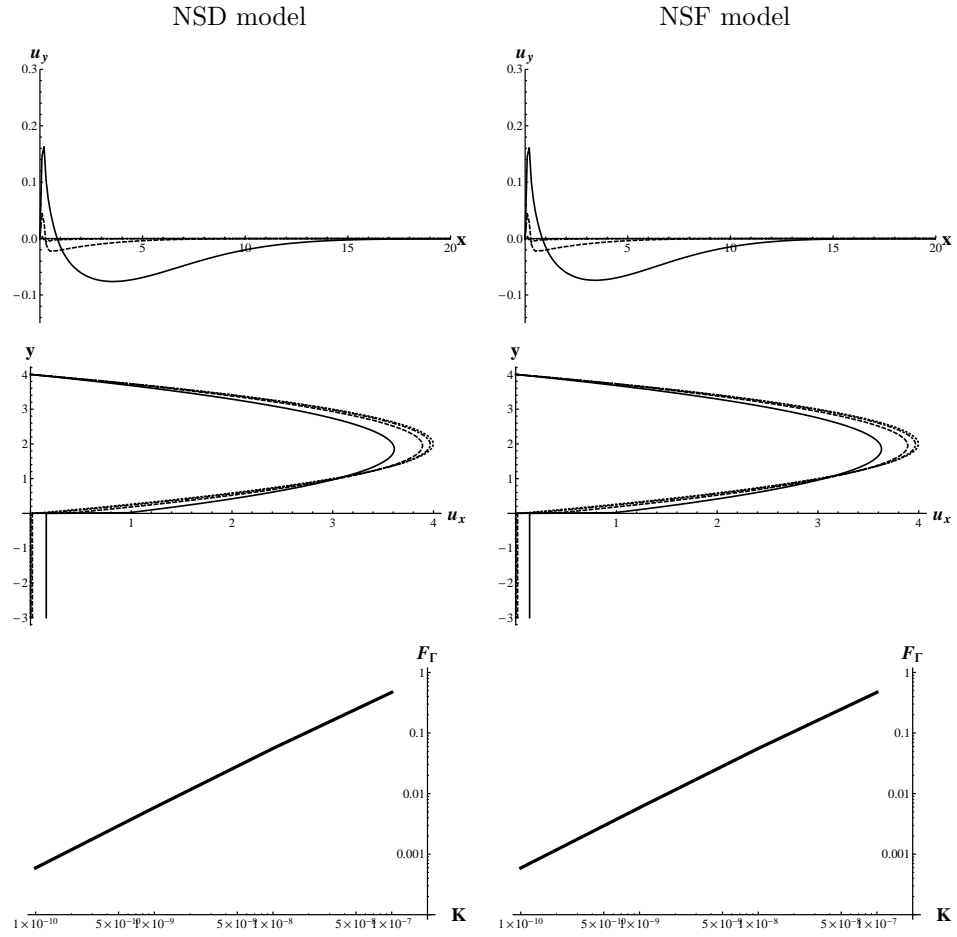


Figure 10: Comparison between the normal component of the velocity across the interface (top), the velocity profile at outlet (mid) and the flux entering the porous domain (bottom) computed using either the NSD or the NSF model with K equal to 10^{-7} (solid line), 10^{-8} (dashed line), 10^{-9} (dot-dashed line) and 10^{-10} (dotted line).

428 contrast to the jump that characterizes NSD and NSF (see Figure 11). Looking
 429 at the velocity profile obtained by PE, it would be impossible to find out where
 430 the porous medium is placed. Thus, this model does not represent correctly the
 431 macroscopic physical behavior in the contact area with the porous medium.

432 However, outside the transition zone, the PE model compares quite well
 433 with the others. Indeed, at the outlet of the fluid domain, although the peak
 434 velocity is different (since the total flow must be constant), the velocity near the
 435 interface is very close to the one given by NSF or NSD. We can then conclude
 436 that the velocity profile is quite similar, except in the very first layer of the
 437 porous medium.

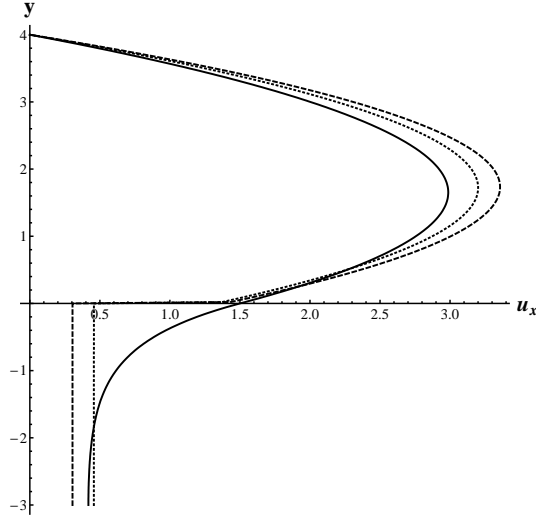


Figure 11: Velocity profile at outlet: solvers comparison (NSD dotted line, NSF dashed line, PE solid line).

438 Observing the normal velocity in Figure 12, we can see that much more flow
 439 enters the porous medium in the case of the PE solver, since the inertial effects
 440 are taken in account not only by the Forchheimer term, but also by the inertial
 441 term of the Navier-Stokes equations.

442 Finally, we study the flux \mathcal{F}_Γ (or equivalently \mathcal{F}_{δ_3}), analyzing its behavior
 443 with respect to the permeability K and the Forchheimer coefficient C_F (in the

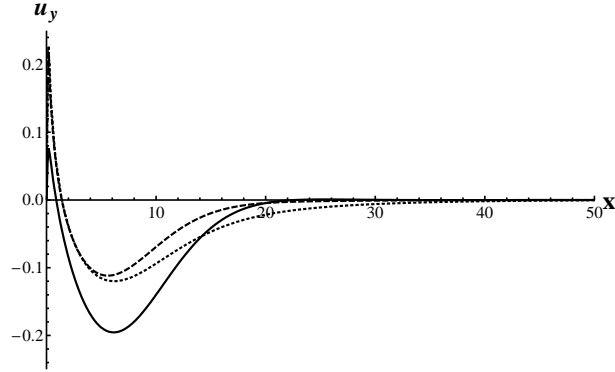


Figure 12: Normal component of the velocity across the interface: solvers comparison (NSD dotted line, NSF dashed line, PE solid line).

444 latter case, we set the permeability to its original value $K = 3.71 \cdot 10^{-7} m^2$.
 445 Figure 13 gives a comparison of its trend for the NSF and PE models. Although
 446 the values do not match, we can observe that all the curves display the same
 447 trends.

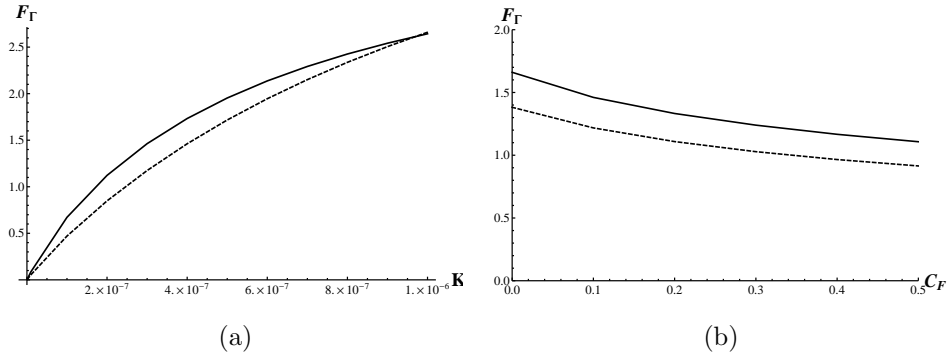


Figure 13: Trend of the flux across the interface for the NSF model (dashed line) and the PE one (solid line), with respect to the permeability K (a) and the Forchheimer coefficient C_F (b).

448 Concerning the computational costs, despite its easiness of implementation
 449 if compared to NSD and NSF, the PE method is more expensive than the other
 450 two. Indeed, PE requires to solve the full Navier-Stokes equations both in Ω_f

451 and Ω_p while NSD and NSF replace them, respectively, by the simpler Darcy
452 or Forchheimer equations in the porous media domain Ω_p .

453 **5. Application to a 3D configuration of internal ventilation of a hel-** 454 **met**

455 In this section we apply the PE approach to study a 3D configuration rep-
456 resenting a schematic test case for the real helmet ventilation problem that
457 motivated this work.

458 The problem of internal ventilation of a motorcycle helmet is associated
459 with the thermal comfort of the rider: a sufficient airflow must be guaranteed
460 to ensure the use of the helmet even in very hot and humid external conditions.
461 For these reasons each helmet has to be equipped with an efficient ventilation
462 system capable of removing as much heat and sweat as possible from the head
463 of the rider. At the moment there is a total lack of fluid-dynamic guidelines
464 for the design of such ventilation systems, which are drawn only according to
465 intuition and experience.

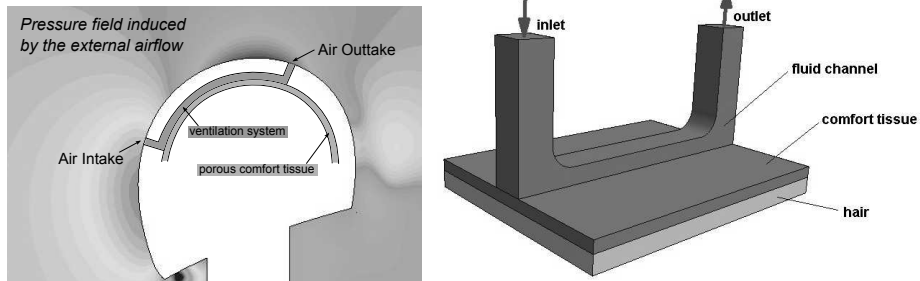


Figure 14: Schematic representation of an internal ventilation system for an helmet (left) and 3D geometry used in numerical simulations.

466 Figure 14 shows a sample geometry of one of such ventilation systems: a
467 channel dug into the protection layer lets the external air enter inside the helmet,
468 leading it directly above the head. The model includes two porous layers (with
469 different permeabilities) in order to represent the comfort tissue attached to the

470 interior of the helmet and the hair of the rider. The airflow is actually induced
471 by the pressure gap between the inlet and the outlet, which is associated with
472 the external shape of the helmet as well as with the velocity of the wind. In a real
473 case, such pressure gradient could be obtained either by direct measurements
474 or by external aerodynamics simulation of the cap alone.

475 Disregarding in a first step the thermal analysis and all the sweat-related
476 issues (we refer the reader to [11]), it is possible to assess the quality of the
477 ventilation system by studying how the airflow is influenced by the geometry
478 of the channels and by the thickness and the physical properties of the porous
479 tissue.

480 For our simulation, the inlet and outlet channels have a square section of edge
481 6 mm and their height is 23 mm . The distance between the channels is 50 mm ,
482 while the extension of the porous layers in the transversal direction is 40 mm .
483 The porous domain is made of a 2 mm thick comfort tissue with permeability
484 $K_p = 5 \cdot 10^{-8}\text{ m}^2$ and Forchheimer coefficient $C_{F,p} = 0.34$, and of the hair
485 layer supposed of 3 mm thickness, with permeability $K_h = 7.5 \cdot 10^{-7}\text{ m}^2$ and
486 Forchheimer coefficient $C_{F,h} = 0.5$. (The data used in this simulation have been
487 obtained within a collaboration with an industrial partner. For more details we
488 refer to [16].) An unstructured tetrahedral mesh of about 32000 elements has
489 been generated using freeFEM++.

490 We impose a pressure drop of 0.1 Pa between inlet and outlet. We refer to
491 [6, 16] on how to include this boundary condition in the weak formulation. On
492 the remaining boundaries we impose a zero airflow condition.

493 Figures 15, 16 and 17 show the behavior of the airflow inside the computa-
494 tional domain. In particular, focusing on the medial section, it is possible to
495 see that the seepage velocity is higher on the hair than on the comfort tissue
496 (which has a lower permeability), meaning that the air moves across the latter
497 one and circulates beneath where it encounters a lower resistance.

498 Finally, we can estimate the mass flow rate of this simple ventilation system
499 by computing the surface integral of the vertical component of the velocity on
500 the inlet (or on the outlet), which turns out to be $2.44 \cdot 10^{-3}\text{ m}^3/\text{s}$. The mass

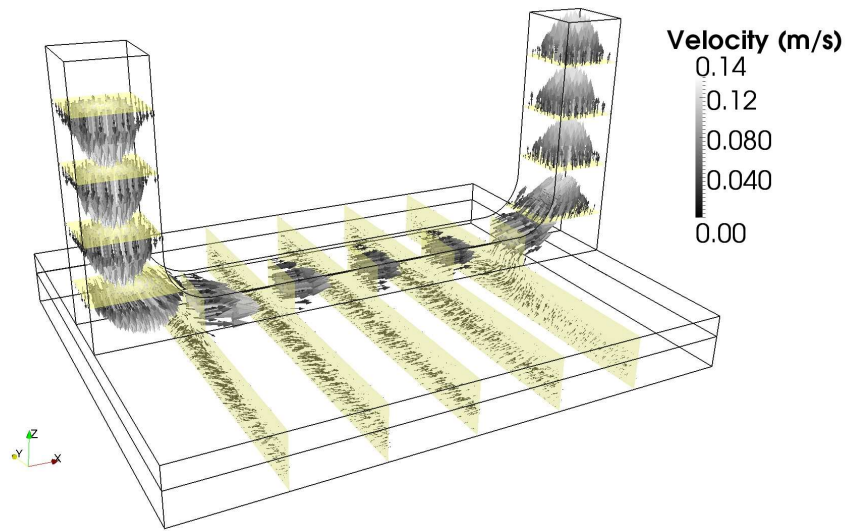


Figure 15: Velocity field across some vertical and horizontal sections of the domain.

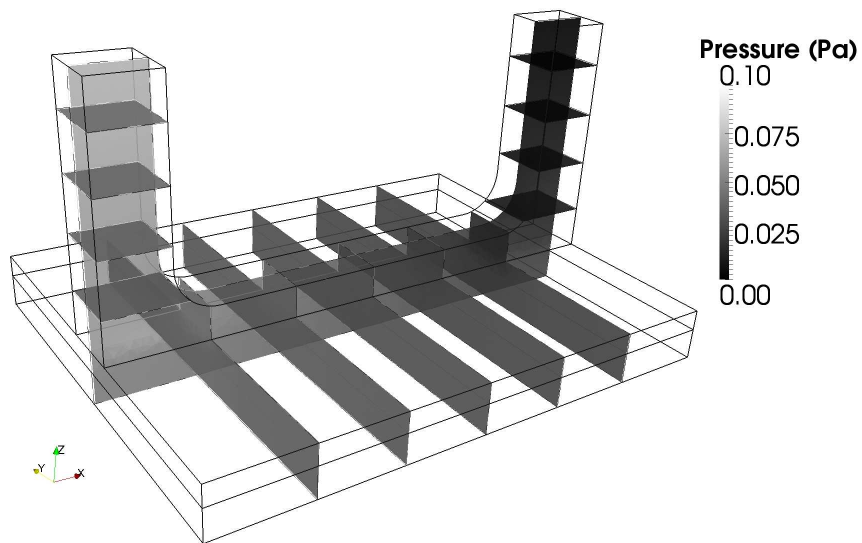


Figure 16: Pressure field across some vertical and horizontal sections of the domain.

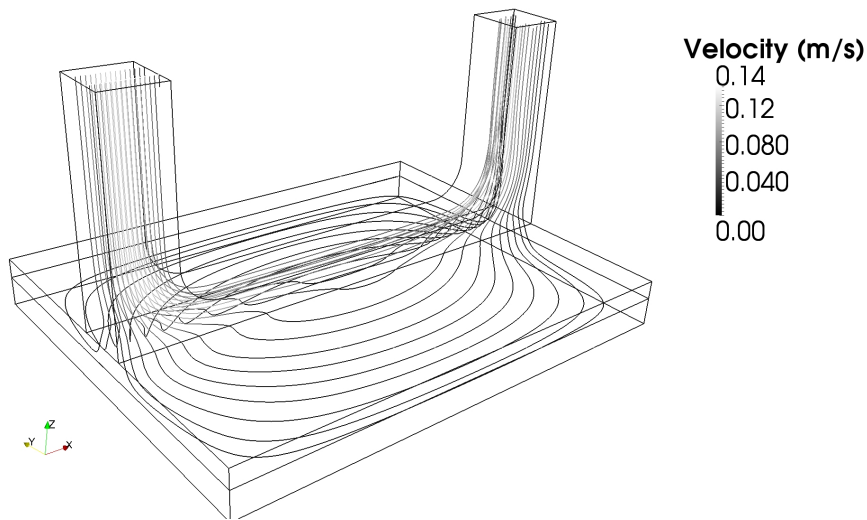


Figure 17: Streamlines colored by velocity magnitude.

501 flow rate could be considered as objective function in an optimization framework
 502 aiming at optimizing the physical properties of the porous layer or the shape of
 503 the air channels. This issue will be the object of a future work.

504 6. Conclusions

505 We have presented different approaches for modeling incompressible flows
 506 in a domain partially occupied by a porous medium. In particular, we have
 507 considered models with different equations in the two subregions of the domain
 508 coupled via interface conditions (NSD and NSF), and a unified approach (PE)
 509 where the presence of the porous region is described by suitable coefficients of
 510 the same equation. We have proposed an iterative algorithm to compute the sta-
 511 tionary solution of the NSD and NSF models and discussed its implementation.
 512 Finally, we have shown an application of the PE method to the computation of
 513 the air flow for the internal ventilation of a motorcycle helmet.

514 We can conclude that, on one hand, the NSF model allows to represent care-
 515 fully the physics of the problem since it permits to precisely locate the interface

516 and it features ad-hoc models for each subregion. However, its implementation
517 is rather complex and its solution requires ad-hoc algorithms whose convergence
518 properties may vary sensibly depending on the considered problem.

519 On the other hand, the penalized model can be straightforwardly imple-
520 mented in a code already developed for the solution of the Navier-Stokes equa-
521 tions, but it cannot represent correctly the physical behavior of the fluid, espe-
522 cially in the first layers of the porous domain.

523 However, from the macroscopic viewpoint the results obtained with these
524 models are not dramatically different. In many engineering applications where a
525 careful description of the flow at the interface between fluid and porous medium
526 is not required, like in the example of internal ventilation of Section 5, the
527 penalization approach can thus provide results similar to those obtained by the
528 coupled methods with less programming effort.

529 **Acknowledgments.** The second author acknowledges the partial support
530 of the Marie Curie Career Integration Grant 2011-294229 within the 7th Euro-
531 pean Community Framework Programme.

532 References

- 533 [1] P. Angot, Analysis of singular perturbations on the Brinkman problem for
534 fictitious domain models of viscous flows, *Math. Methods Appl. Sci.* 22
535 (1999) 1395–1412.
- 536 [2] Ansys CFX, CFX-Solver: Theory, 2005.
- 537 [3] L. Badaea, M. Discacciati, A. Quarteroni, Numerical analysis of the Navier-
538 Stokes/Darcy coupling, *Numer. Math.* 115 (2010) 195–227.
- 539 [4] J. Bear, *Hydraulics of Groundwater*, McGraw-Hill, New York, 1979.
- 540 [5] G. Beavers, D. Joseph, Boundary conditions at a naturally permeable wall,
541 *J. Fluid Mech.* 30 (1967) 197–207.

- 542 [6] C. Bègue, C. Conca, F. Murat, O. Pironneau, Les équations de Stokes
543 et de Navier-Stokes avec des conditions aux limites sur la pression, in:
544 Nonlinear partial differential equations and their applications. Collège de
545 France Seminar, Vol. IX (Paris, 1985–1986), volume 181 of *Pitman Res.*
546 *Notes Math. Ser.*, Longman Sci. Tech., Harlow, 1988, pp. 179–264.
- 547 [7] F. Brezzi, M. Fortin, Mixed and Hybrid Finite Element Method, Springer,
548 New York, 1991.
- 549 [8] H. Brinkman, A calculation of the viscous force exerted by a flowing fluid
550 on a dense swarm of particles, *Applied Scientific Research* 1 (1949) 27–34.
- 551 [9] C. Bruneau, I. Mortazavi, Numerical modelling and passive flow control
552 using porous media, *Computers & Fluids* 37 (2008) 488–498.
- 553 [10] E. Burman, P. Hansbo, A unified stabilized method for Stokes’ and Darcy’s
554 equations, *J. Comput. Appl. Math.* 198 (2007) 35–51.
- 555 [11] C. Canuto, F. Cimolin, A sweating model for the internal ventilation of a
556 motorcycle helmet, *Computers and Fluids* 1 (2011) 29–37.
- 557 [12] Y. Cao, M. Gunzburger, F. Hua, X. Wang, Coupled Stokes-Darcy model
558 with Beavers-Joseph interface boundary conditions, *Commun. Math. Sci.*
559 8 (2010) 1–25.
- 560 [13] CD-Adapco, Star-CCM+ User Guide, 2007.
- 561 [14] A. Cesmelioglu, V. Girault, B. Rivière, Time-dependent coupling of Navier-
562 Stokes and Darcy flows, *Math. Model. Numer. Anal.* (2012). To appear.
- 563 [15] Z. Chen, S. Lyons, G. Qin, Derivation of the Forchheimer law via homog-
564 enization, *Transp. Porous Media* 44 (2001) 325–335.
- 565 [16] F. Cimolin, Analysis of the Internal Ventilation for a Motorcycle Helmet,
566 Ph.D. thesis, Politecnico di Torino, 2010.

- 567 [17] C. D'Angelo, P. Zunino, A finite element method based on weighted interior
568 penalties for heterogeneous incompressible flows, *SIAM J. Numer. Anal.* 47
569 (2009) 3990–4020.
- 570 [18] H. Darcy, *Les Fontaines Publiques de la Ville de Dijon*, Dalmont, Paris,
571 1856.
- 572 [19] M. Discacciati, *Domain Decomposition Methods for the Coupling of Surface
573 and Groundwater Flows*, Ph.D. thesis, Ecole Polytechnique Fédérale de
574 Lausanne, Switzerland, 2004.
- 575 [20] M. Discacciati, E. Miglio, A. Quarteroni, Mathematical and numerical
576 models for coupling surface and groundwater flows, *Appl. Numer. Math.*
577 43 (2002) 57–74.
- 578 [21] M. Discacciati, A. Quarteroni, Navier-Stokes/Darcy coupling: modeling,
579 analysis, and numerical approximation, *Rev. Mat. Complut.* 22 (2009) 315–
580 426.
- 581 [22] H. Ene, E. Sanchez-Palencia, Equations et phénomènes de surface pour
582 l'écoulement dans un modèle de milieu poreux, *J. Mécanique* 14 (1975)
583 73–108.
- 584 [23] M. Firdaouss, J.L. Guermond, P. Le Quéré, Nonlinear corrections to
585 Darcy's law at low Reynolds numbers, *J. Fluid Mech.* 343 (1997) 331–350.
- 586 [24] Fluent Inc., *Fluent User's Guide*, 2005.
- 587 [25] P. Forchheimer, *Wasserbewegung durch Boden*, *Z. Ver. Deutsch. Ing.* 45
588 (1901) 1782–1788.
- 589 [26] J. Galvis, M. Sarkis, Inf-sup for coupling Stokes-Darcy, in: *XXV Iberian
590 Latin American Congress in Computational Methods in Engineering, 2005*,
591 Recife. *Proceedings of the XXV Iberian Latin American Congress in Com-
592 putational Methods in Engineering, Recife, Brazil, 2004*, Universidade Fed-
593 eral de Pernambuco, 2004.

- 594 [27] J. Galvis, M. Sarkis, Balancing domain decomposition methods for mor-
595 tar coupling Stokes-Darcy systems, in: Domain decomposition methods in
596 science and engineering XVI, volume 55 of *Lect. Notes Comput. Sci. Eng.*,
597 Springer, Berlin, 2007, pp. 373–380.
- 598 [28] J. Galvis, M. Sarkis, BDD and FETI methods for mortar coupling of Stokes-
599 Darcy, Technical Report Serie A 563, Instituto Nacional de Matemática
600 Pura e Aplicada, Brazil, 2007.
- 601 [29] J. Galvis, M. Sarkis, Non-matching mortar discretization analysis for the
602 coupling Stokes-Darcy equations, *Electron. Trans. Numer. Anal.* 26 (2007)
603 350–384.
- 604 [30] G. Gatica, R. Oyarzúa, F.J. Sayas, Convergence of a family of Galerkin
605 discretizations for the Stokes-Darcy coupled problem, Technical Report 08-
606 11, Departamento de Ingeniería Matemática, Universidad de Concepción,
607 2008.
- 608 [31] V. Girault, B. Rivière, DG approximation of coupled Navier-Stokes and
609 Darcy equations by Beaver-Joseph-Saffman interface condition, *SIAM J.*
610 *Numer. Anal.* 47 (2009) 2052–2089.
- 611 [32] V. Girault, M. Wheeler, Numerical discretization of a Darcy-Forchheimer
612 model, *Numer. Math.* 110 (2008) 161–198.
- 613 [33] F. Hecht, O. Pironneau, A. Le Hyaric, K. Ohtsuka, *Freefem++ Manual*,
614 Second Edition, 2008.
- 615 [34] O. Iliev, V. Laptev, On numerical simulation of flow through oil filters,
616 *Comput. Visual. Sci.* 6 (2004) 139–146.
- 617 [35] O. Iliev, D. Vasileva, On a local refinement solver for coupled flow in plain
618 and porous media, in: *Numerical Methods and Applications – 6th Inter-*
619 *national Conference, NMA 2006, Borovets, Bulgaria, August 20-24, 2006.*,
620 *Lecture Notes in Computer Science*, Springer, Berlin and Heidelberg, 2007,
621 pp. 590–598.

- 622 [36] W. Jäger, A. Mikelić, On the boundary conditions at the contact interface
623 between a porous medium and a free fluid, *Ann. Scuola Norm. Sup. Pisa*
624 *Cl. Sci.* 23 (1996) 403–465.
- 625 [37] W. Jäger, A. Mikelić, On the interface boundary condition of Beavers,
626 Joseph and Saffman, *SIAM J. Appl. Math.* 60 (2000) 1111–1127.
- 627 [38] W. Jäger, A. Mikelić, N. Neuss, Asymptotic analysis of the laminar viscous
628 flow over a porous bed, *SIAM J. Sci. Comput.* 22 (2001) 2006–2028.
- 629 [39] K. Khadra, P. Angot, S. Parneix, J. Caltagirone, Fictitious domain ap-
630 proach for numerical modelling of Navier-Stokes equations, *Int. J. Numer.*
631 *Meth. Fluids* 34 (2000) 651–684.
- 632 [40] W. Layton, F. Schieweck, I. Yotov, Coupling fluid flow with porous media
633 flow, *SIAM J. Num. Anal.* 40 (2003) 2195–2218.
- 634 [41] T. Levy, E. Sanchez-Palencia, On the boundary conditions for fluid flow in
635 porous media, *Int. J. Engng. Sci.* 13 (1975) 923–940.
- 636 [42] E. Marušić-Paloka, A. Mikelić, The derivation of a nonlinear filtration law
637 including the inertia effects via homogenization, *Nonlin. Anal.* 42 (2000)
638 97–137.
- 639 [43] M.C. Néel, Convection forcée en milieu poreux: écarts à la loi de Darcy, *C.*
640 *R. Acad. Sci. Paris, Série Iib* 326 (1998) 615–620.
- 641 [44] E.J. Park, Mixed finite element methods for generalized Forchheimer flow
642 in porous media, *Numer. Methods Partial Differential Equations* 21 (2005)
643 213–228.
- 644 [45] L. Payne, B. Straughan, Analysis of the boundary condition at the inter-
645 face between a viscous fluid and a porous medium and related modelling
646 questions, *J. Math. Pures Appl.* 77 (1998) 317–354.
- 647 [46] A. Quarteroni, A. Valli, *Numerical Approximation of Partial Differential*
648 *Equations*, Springer, Berlin, 1994.

- 649 [47] A. Quarteroni, A. Valli, Domain Decomposition Methods for Partial Dif-
650 ferential Equations, Oxford University Press, New York, 1999.
- 651 [48] B. Rivière, I. Yotov, Locally conservative coupling of Stokes and Darcy
652 flows, *SIAM J. Numer. Anal.* 42 (2005) 1959–1977.
- 653 [49] P. Saffman, On the boundary condition at the interface of a porous medium,
654 *Stud. Appl. Math.* 1 (1971) 93–101.
- 655 [50] L. Tartar, Incompressible fluid flow in a porous medium: convergence of the
656 homogenization process, in: *E. Sánchez-Palencia, Non-Homogeneous Me-*
657 *dia and Vibration Theory*, volume 127 of *Lecture Notes in Physics*, Springer,
658 Berlin, 1980, pp. 368–377.
- 659 [51] J. Urquiza, D. N’Dri, A. Garon, M. Delfour, Coupling Stokes and Darcy
660 equations, *Appl. Numer. Math.* 58 (2008) 525–538.
- 661 [52] K. Vafai, S. Kim, On the limitations of the Brinkman-Forchheimer-
662 extended Darcy equation, *Int. J. Heat and Fluid Flow* 16 (1995) 11–15.
- 663 [53] P. Zunino, Mathematical and Numerical Modeling of Mass Transfer in the
664 Vascular System, Ph.D. thesis, Ecole Polytechnique Fédérale de Lausanne,
665 Switzerland, 2002.